The Astrophysical Journal, 801:122 (12pp), 2015 March 10 doi:10.1088/0004-637X/801/2/122

HIGH-PRECISION PHOTOMETRIC REDSHIFTS FROM *SPITZER*/IRAC: EXTREME [3.6] – [4.5] COLORS IDENTIFY GALAXIES IN THE REDSHIFT RANGE $z \sim 6.6 - 6.9$

Renske Smit[1,2], Rychard J. Bouwens[1], Marijn Franx[1], Pascal A. Oesch[3], Matthew L. N. Ashby[4], S. P. Willner[4], Ivo Labbé[1], Benne Holwerda[1], Giovanni G. Fazio[4], and J.-S. Huang[4]
[1] Leiden Observatory, Leiden University, NL-2300 RA Leiden, Netherlands
[2] Centre for Extragalactic Astronomy, Durham University, South Road, Durham, DH1 3LE, UK
[3] Yale Center for Astronomy and Astrophysics, Yale University, New Haven, CT 06520, USA
[4] Harvard-Smithsonian Center for Astrophysics, 60 Garden Street, Cambridge, MA 02138, USA
Received 2014 September 17; accepted 2015 January 14; published 2015 March 12

ABSTRACT

One of the most challenging aspects of studying galaxies in the $z \gtrsim 7$ universe is the infrequent confirmation of their redshifts through spectroscopy, a phenomenon thought to occur from the increasing opacity of the intergalactic medium to Lyα photons at $z > 6.5$. The resulting redshift uncertainties inhibit the efficient search for [C II] in $z \sim 7$ galaxies with sub-millimeter instruments such as ALMA, given their limited scan speed for faint lines. One means by which to improve the precision of the inferred redshifts is to exploit the potential impact of strong nebular emission lines on the colors of $z \sim 4 - 8$ galaxies as observed by *Spitzer*/IRAC. At $z \sim 6.8$, galaxies exhibit IRAC colors as blue as $[3.6] - [4.5] \sim -1$, likely due to the contribution of [O III]+Hβ to the 3.6 μm flux combined with the absence of line contamination in the 4.5 μm band. In this paper we explore the use of extremely blue $[3.6] - [4.5]$ colors to identify galaxies in the narrow redshift window $z \sim 6.6 - 6.9$. When combined with an *I*-dropout criterion, we demonstrate that we can plausibly select a relatively clean sample of $z \sim 6.8$ galaxies. Through a systematic application of this selection technique to our catalogs from all five CANDELS fields, we identify 20 probable $z \sim 6.6 - 6.9$ galaxies. We estimate that our criteria select the ~50% strongest line emitters at $z \sim 6.8$ and from the IRAC colors we estimate a typical [O III]+Hβ rest-frame equivalent width of 1085 Å for this sample. The small redshift uncertainties on our sample make it particularly well suited for follow-up studies with facilities such as ALMA.

Key words: galaxies: evolution – galaxies: formation – galaxies: high-redshift

1. INTRODUCTION

Since the installation of the Wide Field Camera 3 (WFC3) on the *Hubble Space Telescope (HST)*, numerous ultraviolet (UV) bright galaxies in the reionization era have been detected through their broadband photometric properties. These observations allow for the determination of the UV luminosity function (e.g., Bouwens et al. 2011; Lorenzoni et al. 2011; Bowler et al. 2012, 2014; Bradley et al. 2012; Oesch et al. 2012, 2013, 2014; McLure et al. 2013; Schenker et al. 2013a) and the typical UV colors of galaxies out to $z \sim 8$ (Stanway et al. 2005; Bouwens et al. 2009, 2012, 2013; Wilkins et al. 2011; Dunlop et al. 2012, 2013; Finkelstein et al. 2012).

In contrast to the success of identifying candidate galaxies out to $z \sim 8$ with *HST*/WFC3 imaging, confirming the redshift of these sources with spectroscopy has proven very challenging due to the absorption of Lyα photons by the neutral Intergalactic Medium (IGM) at $z \gtrsim 6.5$ (Pentericci et al. 2011; Finkelstein et al. 2013; Treu et al. 2013; Caruana et al. 2014; Schenker et al. 2014; Vanzella et al. 2014). This creates particular challenges for follow-up studies with the newest generation of sub-millimeter telescopes such as ALMA. ALMA has the potential to perform detailed studies of star formation rates (SFRs), kinematic structure, and energetics of $z \sim 6 - 8$ galaxies through the direct detection of sub-millimeter fine structure lines such as [C II]λ157.7 μm (e.g., Carilli & Walter 2013). However, the frequency range that ALMA is able to scan in one tuning is relatively small, making follow-up studies with ALMA on sources without accurate redshift information observationally expensive.

One way to make progress in this area involves a search for the C III]λ1908 Å line in $z \gtrsim 6$ galaxies (Stark et al. 2014a, 2014b). This line has a typical rest-frame equivalent width (EW_0) of ~4–14 Å in two $z \sim 6 - 7$ galaxies where this line has been successfully located (Stark et al. 2014b) and in low-mass lensed star-forming galaxies at $z \sim 2$ (Stark et al. 2014a). The challenge with this approach is the faintness of the CIII] line and high density of sky lines in many regions of the near-infrared (IR) spectrum.

Another potentially promising way forward is to utilize the information provided by the *Spitzer*/IRAC. Recent studies have reported evidence for the presence of strong nebular emission lines such as Hα and [O III]λ5007 Å through the apparent impact of these lines on the IRAC 3.6 and 4.5 μm fluxes of $z \sim 4 - 8$ galaxies (Schaerer & de Barros 2009; Shim et al. 2011; González et al. 2012, 2014; Labbé et al. 2013; Stark et al. 2013; Smit et al. 2014). These lines appear to cause the $[3.6] - [4.5]$ colors of high redshift galaxies to vary significantly as a function of redshift. This results in modestly blue $[3.6] - [4.5]$ colors in $z \sim 6$ galaxies, where both bands are contaminated by emission lines, very blue $[3.6] - [4.5]$ colors at $z \sim 6.8$, where only the 3.6 μm band suffers line contamination, and red $[3.6] - [4.5]$ colors for sources at redshifts $z > 7$, where the 4.5 μm band is contaminated (Labbé et al. 2013; Wilkins et al. 2013; Laporte et al. 2014; Smit et al. 2014).

In this paper we attempt to exploit the extreme IRAC colors galaxies exhibit at specific redshifts to isolate galaxies over a narrow range in redshift. To test this method, we utilize a large sample of $z \sim 5 - 8$ galaxies identified from the CANDELS program (Grogin et al. 2011; Koekemoer et al. 2011). We

select a sample of sources with extremely blue [3.6] – [4.5] IRAC colors and show that these sources likely fall in the narrow redshift range $z\sim$ 6.6 – 6.9. Ultimately, of course, this approach and the assumptions behind it will need to be tested through spectroscopy with the *James Webb Space Telescope (JWST)*.

Additionally we discuss a few objects with blue [3.6] − [4.5] colors that are clearly at $z \lesssim 6.6$ from their *HST* photometry, and we suggest that these objects could be explained by high [O III]/Hβ ratios such as found at $z \sim 3$ (Schenker et al. 2013b; Holden et al. 2014).

This paper is organized as follows. Section 2 discusses our data set and photometric procedure. Section 3 presents the [3.6] − [4.5] IRAC colors as a function of photometric redshift for a sample of $z \sim 5 - 8$ UV-selected galaxies. Section 4 discusses the selection of extreme [3.6] − [4.5] color galaxies, and Section 5 presents our $z \sim$ 6.6 – 6.9 galaxy sample. Section 6 gives a short summary of our results.

Throughout this paper we adopt a Salpeter IMF with limits 0.1–100 $M_{\odot}$ (Salpeter 1955). For ease of comparison with previous studies we take $H_0 = 70 \mathrm{kms}^{-1}\,\mathrm{Mpc}^{-1}$, $\Omega_m = 0.3$, and $\Omega_\Lambda = 0.7$. Magnitudes are quoted in the AB system (Oke & Gunn 1983)

2. OBSERVATIONS, PHOTOMETRY AND $z \sim$ 5 – 8 SAMPLE

2.1. HST Data and Photometry

The primary sample of $z \sim 5 - 8$ galaxies that we use in this paper was selected from the catalogs described by Bouwens et al. (2014). The purpose of this sample is to establish how the [3.6] − [4.5] color of galaxies depends on redshift and also to establish the redshift distribution of galaxies with the most extreme IRAC colors. The catalogs were compiled from *HST* Advanced Camera for Surveys (ACS) (B_{435}, V_{606}, i_{775}, I_{814} and z_{850}) and WFC3/IR (Y_{098}/Y_{105}, J_{125}, JH_{140} and H_{160}) data over the GOODS-N and GOODS-S fields. We also used the deep and wide-area observations obtained in the HUDF09+HUDF12 (Beckwith et al. 2006; Bouwens et al. 2011; Ellis et al. 2013; Illingworth et al. 2013), ERS (Windhorst et al. 2011), and CANDELS (Grogin et al. 2011; Koekemoer et al. 2011) programs as well as any archival *HST* observations over these fields. The shallow JH_{140} imaging was taken from the 3D-*HST* survey (Brammer et al. 2012a) and A Grism Hα Spectroscopic survey (PI:Weiner). The procedure for reducing the data is described in detail by Illingworth et al. (2013) and Bouwens et al. (2014).

A secondary sample of $z \sim 5 - 8$ galaxies is used to increase the number of $z \sim 6.8$ and $z \sim 6.0$ galaxies in our selection. We derived this sample from the *HST* data over the CANDELS-UDS, CANDELS-COSMOS, and CANDELS-EGS fields (V_{606}, I_{814}, J_{125} and H_{160}, for more details on the CANDELS fields see Koekemoer et al. 2011 and Skelton et al. 2014) and deep *U*- and *B*-band ground-based observations from Canada–France–Hawaii Telescope and Subaru (Capak et al. 2007; Furusawa et al. 2008).

An overview of all fields, bands and depths is given in Table 1 of Bouwens et al. (2014). Both the ACS and WFC3/IR data reach total magnitudes of $\gtrsim$27.2 at 5σ, using as a basis the flux uncertainties on the total magnitude measurements for the faintest 20% of galaxies from the Bouwens et al. (2014) catalogs over these fields. Our total search area over all the fields is 720 arcmin^2.

The photometry followed the procedure described by Bouwens et al. (2012). In short, we ran an adapted version of the Source Extractor software (Bertin & Arnouts 1996) in dual-image mode. The detection images were created by combining all deep bands redwards of the Lyman break (i.e., Y_{098}/Y_{105}, J_{125}, and H_{160}) into a square-root χ^2 image (Szalay et al. 1999). After matching the observations to the H_{160}-band point-spread function (PSF), colors and total magnitudes were measured in Kron-like apertures with Kron factors 1.6 and 2.5 respectively (defined on the H_{160}-band).

2.2. Spitzer/IRAC Data and Photometry

The first part of our *Spitzer*/IRAC data set covers all five CANDELS fields with the 3.6 and 4.5 μm bands[5] from the *Spitzer* Extended Deep Survey (PI: Fazio) and all available archival data sets from before 2011 (Ashby et al. 2013). We complement this data set with the new deep IRAC imaging from the *Spitzer* Very Deep Survey (S-CANDELS) Exploration Science Project (Ashby et al. 2015), which brings the IRAC coverage up to 50 hr in depth (26.8 mag at 5σ in the 3.6 μm band). For the sources in the HUDF, we utilize additional data from the IRAC Ultra Deep Field (Labbé et al. 2013) program.

Before performing photometry on the sources in our sample, we removed the contamination of foreground sources with an automated cleaning procedure (Labbé et al. 2010a, 2010b). In short, the *HST* images provided a high-spatial resolution template with which to model the positions and flux profiles of the foreground sources. The light profiles of individual sources in the *HST* image were convolved with a kernel to match the IRAC PSF and then simultaneously fitted to the IRAC image within a region of ∼11arcsec around the sources from our sample. We subtracted the flux from the foreground galaxies and performed photometry in 2.″0-diameter circular apertures on the resulting images. We applied a correction to account for the flux outside of the aperture, given by the ratio of the flux enclosed in the photometric aperture in the *HST* image (before convolution) to the IRAC model (after convolution). This correction ranges from ∼2.2× to ∼2.4×, depending on the size of the source. The local noise was estimated from the clean background on a residual IRAC image from which all sources were subtracted. Our procedure for deblending can fail when contaminating sources are too bright or too close to the central source. We removed sources from our sample with a high χ^2 parameter determined from the residual IRAC image (see Section 2.3).

2.3. Base Sample of $z \sim 5 - 8$ Galaxies

In this section, we present the base sample of $z \sim 5 - 8$ galaxies we use to study how the IRAC colors of star-forming galaxies depend upon redshift. We selected our sources from which we measure IRAC colors in the rest-frame UV, adopting the Lyman-break technique (Steidel et al. 1999) with the requirement that the source drops out in the I_{814} band. Specifically, our requirements for $z \sim 5 - 8$ Lyman Break

[5] http://irsa.ipac.caltech.edu/data/SPITZER/docs/irac/calibrationfiles/spectralresponse/

Galaxies (LBGs) were

$$(I_{814} - J_{125} > 0.8) \wedge (J_{125} - H_{160} < 0.4)$$
$$\wedge (I_{814} - J_{125} > 2(J_{125} - H_{160}) + 0.8), \quad (1)$$

where $\wedge$ indicates logical AND. We chose the I_{814} and J_{125} band fluxes for our identification of $z \gtrsim 5$ LBGs, instead of more closely spaced passbands like z_{850} and Y_{105}, which are available over the GOODS-N and GOODS-S fields. While this is less optimal for selecting a sample of galaxies with the lowest contamination rate, these bands were chosen in order to select galaxies over a relatively extended redshift range $z \sim 5.5 - z \sim 8.5$ (without any gaps) and to use filters that are available over all five CANDELS fields for a more uniform selection. Information from the more closely spaced bandpasses was nevertheless utilized in deriving photometric redshifts for sources from our selection and hence determining the relationship between the IRAC colors of sources and their redshifts.

We also required sources to have either a non-detection in the V_{606} band ($<2\sigma$) or to have a very strong Lyman break, i.e., $V_{606} - J_{125} > 2.5$. Furthermore, we required sources to be undetected ($<2\sigma$) in the available B_{435}-band data over GOODS north and south or, in the case of the CANDELS UDS, COSMOS, or EGS fields, to be undetected ($<2.5\sigma$) in the χ^2 statistic image Bouwens et al. (2014) derived from the ground-based U and B images. We required the SExtractor stellarity parameter (equal to 0 and 1 for extended and point sources, respectively) in the J_{125} band be less than 0.92 to ensure that our selection is largely free of contamination by stars (e.g., Holwerda et al. 2014). Moreover, the blue IRAC color criterion introduced in Section 2.3 also selects effectively against contamination from brown dwarfs in our Milky Way (Kirkpatrick et al. 2011; B. W. Holwerda et al. 2015, in preparation). We selected sources with a signal-to-noise ratio (S/N) $\mathrm{S/N}(H_{160}) > 5$, and additionally we required $f_\nu(H_{160})/ef_\nu(3.6\,\mu\mathrm{m}) > 2.5$ and $f_\nu(H_{160})/ef_\nu(4.5\,\mu\mathrm{m}) > 2.5$, where $f_\nu(H_{160})$ is the measured flux density in the H_{160} band and $ef_\nu(3.6\ \mu\mathrm{m})$ and $ef_\nu(4.5\ \mu\mathrm{m})$ are the estimated uncertainties in the 3.6 and 4.5 μm band fluxes. Our chosen requirements explicitly do not include a dependence on the observed flux in the IRAC bands to ensure that our results are not biased according to the emission line flux in our candidates. In practice, most high-redshift sources exhibit a somewhat red UV-to-optical color (González et al. 2012), and as a result 75% of our sample is detected at $>5\sigma$ in the 3.6 μm IRAC band. We exclude those ~30% of the sources that show strong residuals in the IRAC images after our deblending procedure (Section 2.2), which results in a final sample of 220 sources in GOODS-N/S and 224 sources in CANDELS-EGS/UDS/COSMOS.

3. [3.6] − [4.5] COLOR VERSUS REDSHIFT

Before moving onto a discussion of how the IRAC [3.6] − [4.5] color might be used to refine redshift determinations for specific $z > 6$ selections, it is useful to quickly assess whether our sample agrees with our main assumption: that the [3.6] − [4.5] color is strongly influenced by the presence of strong nebular emission lines such as Hα and [O III] in the IRAC filters. To this end we explore the variation of the median [3.6] − [4.5] color as a function of redshift for our sample.

Figure 1 shows the colors of our GOODS-N/S sample as a function of the photometric redshift, as derived from the *HST* broadband photometry. We used the software Easy and Accurate Zphot from Yale (EAZY; Brammer et al. 2008) to estimate photometric redshifts for the galaxies in our sample. We used the standard template set of EAZY, but we complemented these templates with a number of templates generated with Galaxy Evolutionary Synthesis Models (GALEV; Kotulla et al. 2009), which includes nebular continuum and emission lines as described by Anders & Fritze-v. Alvensleben (2003). Additionally we included a template with an [OIII]λ4959,5007Å/Hβ ratio of 10 to match the most extreme line ratios observed in spectroscopy of galaxies at lower redshifts (Amorín et al. 2012; Brammer et al. 2012b; Jaskot & Oey 2013; Schenker et al. 2013b; van der Wel et al. 2013; Holden et al. 2014; Steidel et al. 2014). No use of the *Spitzer*/IRAC photometry is made in the photometric redshift determination to avoid coupling between our redshift estimates and the measured IRAC fluxes. We do not include sources from our EGS/UDS/COSMOS sample in Figure 1 because of the lack of deep *HST* coverage in the z_{850} and Y_{105}/Y_{098} bands, which is needed for obtaining sufficiently accurate redshifts for the analysis we describe.

We observe a clear discontinuity in the median color (red points) around $z \sim 7$, where the [O III] emission line moves from the 3.6 μm to the 4.5 μm band. Moreover, we find the bluest median [3.6] − [4.5] color at $z \sim 6.8$, where [O III] boosts the 3.6 μm flux while Hα has already moved out of the 4.5 μm band. This suggests that the IRAC colors are strongly influenced by emission lines, in agreement with recent studies (Schaerer & de Barros 2009; Shim et al. 2011; González et al. 2012, 2014; Labbé et al. 2013; Stark et al. 2013; Smit et al. 2014) and in agreement with predictions of stellar population synthesis models with emission lines. We can use this information to improve our determinations of the redshift probability functions for strong line emitters by including the IRAC fluxes in our photometric redshift estimates.

4. ULTRA-BLUE [3.6] − [4.5] GALAXIES

In the previous section we showed how the [3.6] − [4.5] IRAC color would likely change as the [O III] and Hα nebular lines move in and out of the photometric bands, due to the redshifting spectrum. We can use this information to significantly improve our photometric redshift estimates. In particular the IRAC [3.6] − [4.5] color can provide a valuable constraint in sources that have uncertain photometric redshifts from their *HST* photometry, such as sources over COSMOS, UDS, or EGS where only 4 *HST* bands are available. This is important due to the considerable challenges involved in improving redshift estimates through spectroscopy (largely due to the impact of the more neutral IGM on the prevalence of Lyα emission in $z > 6.5$ galaxies). In this section we will investigate a [3.6] − [4.5] color selection on our sample of $z \sim 5 - 8$ galaxies over the GOODS-N and GOODS-S, where good photometric redshift constraints are available and in Section 5 we will present a sample of $z \sim 6.6 - 6.9$ galaxies over all five CANDELS fields.

4.1. *Blue* [3.6] − [4.5] *Sources at* $z \sim 6.8$

A particularly interesting redshift interval is $z \sim 6.6 - 6.9$, where we expect extreme [3.6] − [4.5] colors due to the presence of the [O III] line in the 3.6 μm band and the absence of any strong emission lines in the 4.5 μm band. This is

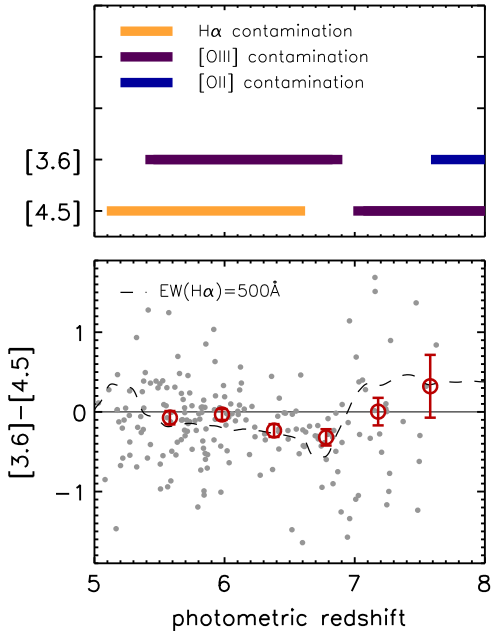

Figure 1. Top panel: a schematic overview of the redshift range where the strongest nebular lines (Hα, [O III] and [O II]) can contaminate the rest-frame optical flux in the 3.6 and 4.5 μm bands. Bottom panel: measurements of the [3.6] − [4.5] color (gray points) in UV-selected galaxies from GOODS-N/S, placed at their photometric redshift. The red points indicate the median colors in $\Delta z = 0.4$ redshift bins (error bars represent the uncertainty in the median, i.e., $\sigma/\sqrt{N}$). The black dashed line provides an example of the IRAC color at different redshifts for a source with flat continuum and $EW_0(H\alpha) = 500$ Å in combination with emission line ratios as defined by Anders & Fritze-v. Alvensleben (2003) for sub-solar metallicity $Z = 0.2\,Z_\odot$. The overall blue [3.6] − [4.5] colors at $z < 7$, vs. red [3.6] − [4.5] colors at $z > 7$ indicate that in particular the presence of [O III] in the IRAC bands might have a significant impact on the [3.6] − [4.5] color.

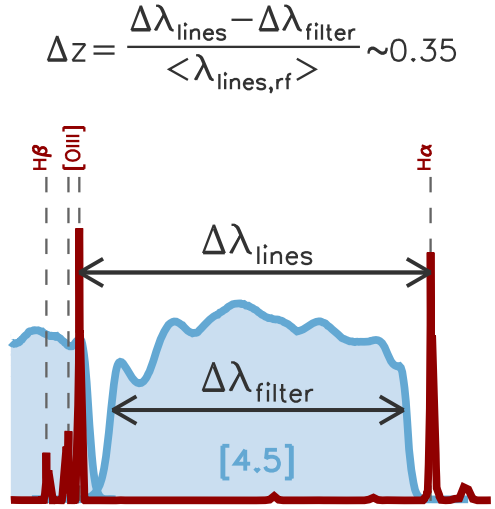

Figure 2. An illustration of the position of the optical nebular emission lines in a $z \sim 6.8$ star-forming galaxy (red line) with respect to the *Spitzer*/IRAC response function (indicated in blue). Our strategy for selecting star-forming galaxies in the narrow redshift range $z \sim 6.6$ – 6.9 capitalizes on the [O III] and Hα emission lines being separated by almost the same wavelength difference as the width of *Spitzer*/IRAC 4.5 μm band. Our [3.6] − [4.5] selection technique furthermore requires that the [O III] line has not yet dropped out of the 3.6 μm band, which narrows the redshift window where we expect to find these ultra-blue galaxies, from $\Delta z \sim 0.35$ to $\Delta z \sim 0.25$.

illustrated in Figure 2. Because the Hα to [O III] line separation ($\Delta\lambda_{\rm lines}$) at $z = 6.8$ is slightly wider than the 4.5 μm filter width ($\Delta\lambda_{\rm filter}$), there is very narrow redshift range $\Delta z = \left(\Delta\lambda_{\rm lines} - \Delta\lambda_{\rm filter}\right)\Big/\left\langle \lambda_{\rm lines,rest-frame} \right\rangle = 0.35$ in which the 4.5 μm band is free of strong emission lines. In practice, the effective redshift range where we can observe the extremely blue IRAC colors is even narrower than this, i.e., $\Delta z \sim 0.25$, because the relevant wavelength is where [O III] leaves the 3.6 μm filter, not where this line enters the 4.5 μm filter (see the top panel of Figure 1).

To investigate whether the selection of sources with blue [3.6] − [4.5] colors can be used to unambiguously identify galaxies at $z \sim 6.8$, we collected a sample of emission line candidate galaxies by selecting sources with [3.6] − [4.5] colors significantly bluer than −0.5 mag. We adopted the criterion

$$P([3.6] - [4.5] < -0.5) > 84\%. \quad (2)$$

This criterion indicates that the sources in our selection have a probability (P) of at least 84% to have a true IRAC color bluer than [3.6] − [4.5] < −0.5, based on the uncertainties in the 3.6 and 4.5 μm fluxes. We show the galaxies meeting this color criterion in Figure 3. A color cut in the [3.6] − [4.5] color can identify galaxies with strong emission lines in the redshift range $z \sim 6.6$ – 6.9, but a galaxy with more moderate emission lines and very blue continuum [3.6] − [4.5] colors can also meet the criterion.

We purposely decided to try to select $z \sim 6.8$ galaxies based on a color criterion rather than fitting emission line templates to the IRAC bands to obtain photometric redshifts. This was done to avoid a dependence on the spectral energy distribution (SED) template set and the assumed line ratios in these templates. Since the physical properties of the H II regions in star-forming galaxies, such as gas metallicity and gas density, strongly influence the line ratios we observe (e.g., Kewley et al. 2013) we wanted to avoid having our results implicitly depend on these ratios.

Over the 270 arcmin^2 CANDELS/ERS region of GOODS-north and GOODS-south, 13 sources satisfy this criterion out of the 220 sources from our base $z \sim 5$ – 8 sample. We indicate these in the top panel of Figure 3 and show a histogram in the bottom panel of Figure 3. Furthermore, there are 15 sources out of 224 sources from the base sample over a 450 arcmin^2 area in the CANDELS-EGS/CANDELS-UDS/CANDELS-COSMOS fields that meet the criterion, but we do not present them in Figure 3 due to the greater difficulty in determining their photometric redshifts.

We identify a large number of blue [3.6] − [4.5] sources that are broadly consistent with a $z \sim 6.8$, similar to the sources found by Smit et al. (2014). For these galaxies the extreme [3.6] − [4.5] colors are explained by the likely scenario that the [O III] emission dominates the 3.6 μm flux while at the same time the 4.5 μm flux is free of emission line contamination. Interestingly enough, Figure 3 indicates there might be a few sources at slightly lower redshift (at $z \sim 6.0$ instead of at $z \sim 6.8$) with such blue IRAC colors; we will discuss these sources in Section 4.2.

Figure 4 shows four examples of blue [3.6] − [4.5] sources in GOODS-N/S that are consistent with a $z \sim 6.8$ from their *HST* photometry only. We present the redshift probability function using only the *HST* bands and also when using constraints from both *Spitzer*/IRAC and *HST*. Due to their

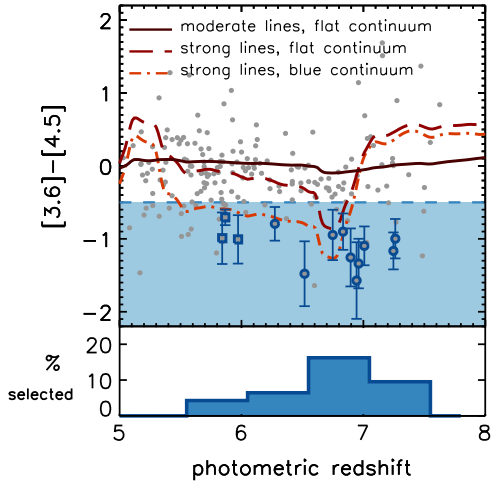

Figure 3. Top panel: measurements of the [3.6] − [4.5] color (gray points) in UV-selected galaxies from GOODS-N/S, placed at their photometric redshift (see also bottom panel of Figure 1). The blue encircled points indicate sources that show IRAC colors significantly bluer than [3.6] − [4.5] < −0.5 (blue shaded area), as given by Equation (2) (the ultra-blue [3.6] − [4.5] colors for many sources in the blue shaded area are not significant). Blue circles indicate sources that are consistent with the redshift range $z \sim 6.6 - 6.9$, while blue squares indicate sources that are at $z < 6.6$ from their photometric redshift probability distribution (99% confidence). The solid lines indicate three tracks of galaxy templates: the dark red solid line indicates a stellar population with moderate emission lines ($EW_{H\alpha,0} \sim 100$ Å) and a flat continuum, the red dashed lines indicates a young (∼5 Myr) stellar population with strong emission lines ($EW_{H\alpha,0} \sim 1000$ Å) and a flat continuum from moderate dust extinction ($E(B-V) \sim 0.2$), while the dotted–dashed orange line indicates a young population with strong emission lines, in combination with a high [O III]/Hβ ratio such as described in Anders & Fritze-v. Alvensleben (2003) for low metallicity gas ($Z = 0.2\,Z_\odot$) and with blue continuum (dust-free). Bottom panel: the percentage of the galaxy population that has blue [3.6] − [4.5] colors, such as defined by Equation (2), at a given photometric redshift. The presence of extremely blue [3.6] − [4.5] colors is most abundant in galaxy candidates at $z \sim 7$.

extreme [3.6] − [4.5] colors we can place very tight constraints on the photometric redshift of these galaxies.

This is particularly useful for follow-up studies to obtain line detections with sub-millimeter detectors such as ALMA. Line detections with interferometer arrays are inherently limited in frequency space by the capabilities of the correlator. ALMA can roughly observe ∼4 GHz in one tuning in band 6 (211–275 GHz).[6] As a reference we indicate the frequency of the bright [C II]λ157.7 μm line at a given redshift in Figure 4 and we indicate the frequency range that ALMA can observe in two frequency tunings. With only twice the observing time required with respect to spectroscopically confirmed sources, we can typically search the ∼95% probability window for [C II] emission in these sources.

The selection of galaxies at $z \sim 6.8$ is also of interest for deriving stellar masses of high-redshift galaxies using *Spitzer*/IRAC constraints (Eyles et al. 2005, 2007; Yan et al. 2005, 2006; Labbé et al. 2006; Stark et al. 2009; Yabe et al. 2009; González et al. 2010, 2011; Labbé et al. 2010b; Curtis-Lake et al. 2013). In particular, the redshift range $z \sim 6.6 - 7.0$ provides us with the only opportunity beyond $z \gtrsim 5.4$ to measure the rest-frame optical stellar continuum without the contamination of nebular line emission in the 4.5 μm band, allowing for more accurate stellar mass and specific SFR estimates (e.g., Smit et al. 2014).

4.2. *Blue* [3.6] − [4.5] *Sources at* $z \sim 6.0$

In the previous section we showed that a large number of sources with ultra-blue [3.6] − [4.5] colors very likely have redshifts in the narrow range 6.6–6.9, where the blue colors can be easily explained by the presence of [O III] in the 3.6 μm band, in contrast to the 4.5 μm band that contains no strong line emission.

Figure 3 also shows a number of very blue [3.6] − [4.5] sources that prefer a redshift around $z \sim 6.0$ and have a probability of less than <1% of being at $z \sim 6.6 - 6.9$ (based on the photometric redshift probability distribution using only *HST* bands). In the redshift range $z \sim 5.4 - 6.6$, [O III] still contaminates the 3.6 μm band, but the strong Hα line also boosts the 4.5 μm flux. Both lines are expected to be strong in young, actively star-forming galaxies, and therefore it is unclear what the explanation is for the significant spread in [3.6] − [4.5] colors and in particular the very blue [3.6] − [4.5] colors observed for a small fraction of the population. While galaxies containing Active Galactic Nuclei can exhibit extremely high [O III]/Hβ ratios, this phenomenon is rare in local galaxies with stellar masses below $M_* < 10^{10}\,M_\odot$ (e.g., Juneau et al. 2013). For our sample of star-forming galaxies at $z \sim 6.0$, with UV-luminosities ranging from $M_{UV} \sim -19$ to $M_{UV} \sim -21$, we expect nearly all sources to have stellar masses below this limit (e.g., González et al. 2011; Salmon et al. 2015). However, we cannot completely rule out this option based on the limited photometric information available for these sources.

Figure 5 shows two examples of sources that are at $z < 6.6$ at high confidence. One source has an IRAC color of [3.6] − [4.5] = −1.0 ± 0.4 but a photometric redshift of $5.84^{+0.25}_{-0.30}$; the other source has an IRAC color of [3.6] − [4.5] = −1.0 ± 0.3 but a photometric redshift of $5.97^{+0.22}_{-0.22}$. In both cases, we clearly cannot use the IRAC colors alone to distinguish between these sources and the sources from Figure 4, which strongly prefer a redshift around $z \sim 6.8$.

One effect that could influence our estimated photometric redshifts for these objects—and possibly offer an explanation for their blue [3.6] − [4.5] colors—is the presence of high EW Lyα emission in these galaxies. For example Schenker et al. (2014) show that a 160 Å EW Lyα line can cause the photometric redshift of a $z \sim 7.5$ galaxy to be underestimated by as much as $\Delta z = 0.2$, suggesting that our blue $z \sim 6.0$ sample may actually be at higher redshift. Though our templates do not include strong Lyα lines, searches for Lyα have shown a low abundance of Lyα emission at $z > 6.5$ (Pentericci et al. 2011; Finkelstein et al. 2013; Treu et al. 2013; Caruana et al. 2014; Schenker et al. 2014), and even at lower redshifts high-EW Lyα is rarely detected in UV bright ($M_{UV} < -20$) galaxies (e.g., Stark et al. 2010). Therefore it seems unlikely to suppose that these blue sources with $z_{phot} \sim 6.0$ are actually $z \sim 6.8$ galaxies with strong Lyα emission.

In order to understand the origin of these extreme IRAC colors at $z \sim 6.0$ we compare the [3.6] − [4.5] color distribution of these sources with the colors we would predict based on a sample of $z \sim 3$ galaxies with near-IR spectroscopy in Figure 6. In the top panel of Figure 6 we show the sub-sample

[6] A. Lundgren, 2013, ALMA Cycle 2 Technical Handbook Version 1.1, ALMA, ISBN 978-3-923524-66-2.

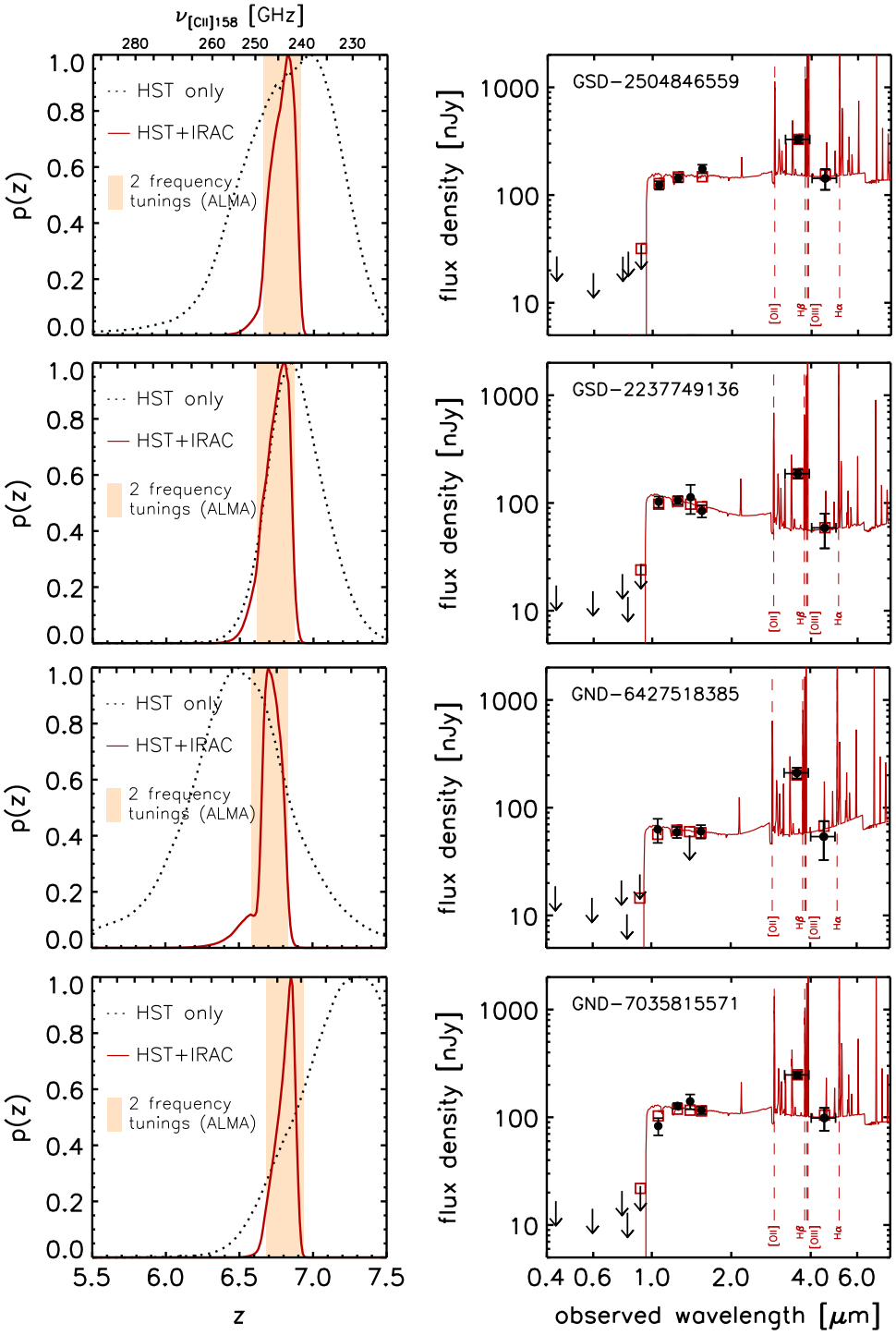

Figure 4. Four examples of sources selected on their blue IRAC colors (Equation (2)) that have a photometric redshift probability distribution consistent (within the 95% confidence interval) with the redshift range $z \sim 6.6$ – 6.9; from top to bottom GSD-2504846559, GSD-2237749136, GND-6427518385, and GND-7035815571 (from the larger Bouwens et al. (2014) catalogs). Left panels: the redshift probability distribution using only the *HST* bands (black dotted line) and using the constraints from both *HST* and *Spitzer*/IRAC (red line). Due to the substantial impact [O III] emission can have on the 3.6 μm flux, the [3.6] − [4.5] color can set tight constraints on the redshifts of individual sources. Two ALMA tunings (indicated with the yellow shaded regions) would be sufficient to obtain a spectroscopic redshift through the [C II]λ158 μm line if one is present within the ∼95% likelihood window. Right panel: Flux densities and 2σ upper limits (black points and arrows) of the *HST* and *Spitzer*/IRAC photometry with the best-fit template (red line). For sources in the redshift window $z \sim 6.6$ – 6.9, the 4.5 μm band is not contaminated by strong emission lines, in contrast with the 3.6 μm band which is dominated by the flux in the [O III] line.

of sources that (with 68% confidence) have a redshift in the range $z \sim 5.4$ – 6.6, where [O III] emission contaminates the 3.6 μm band while at the same time Hα emission contaminates the 4.5 μm band (see the top panel of Figure 1). In the bottom panel of Figure 6 we show a prediction of the [3.6] − [4.5] color distribution from the spectroscopic properties of [O III] and Hβ in $z \sim 3$ LBGs as listed by Schenker et al. (2013b) and Holden et al. (2014). These authors find line ratios as high as [O III]λ4959,5007 Å/Hβ ∼ 10. This strong [O III] flux with respect to the hydrogen Balmer lines could result in very blue

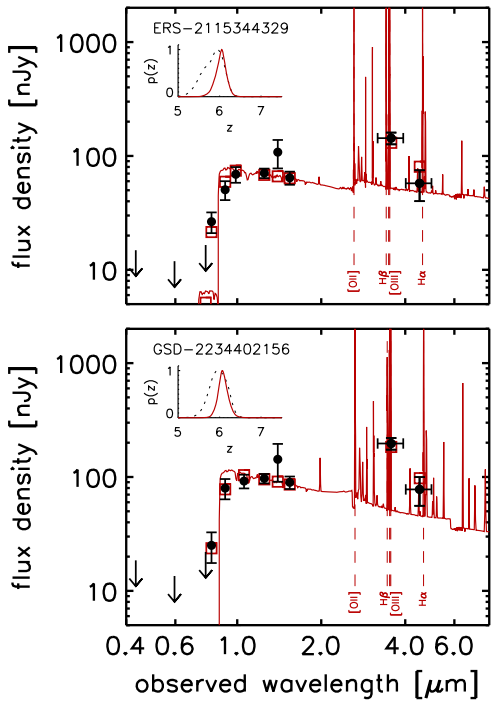

Figure 5. Two examples of sources that prefer a redshift below $z < 6.6$ (ERS-2115344329 and GSD-2234402156) from their photometric redshift distribution (99% confidence), but that also satisfy our [3.6] − [4.5] color criterion (Equation (2)). Flux densities and upper limits (2σ) of the *HST* and *Spitzer*/IRAC photometry are indicated with black points and arrows, while the best-fit template is drawn in red. The 4.5 μm band is contaminated by Hα, while the 3.6 μm band is dominated by the flux in the [O III] line. The inset panel in the top left corner indicates the redshift probability distribution using only the *HST* bands (black dotted line) and using the constraints from both *HST* and *Spitzer*/IRAC (red line).

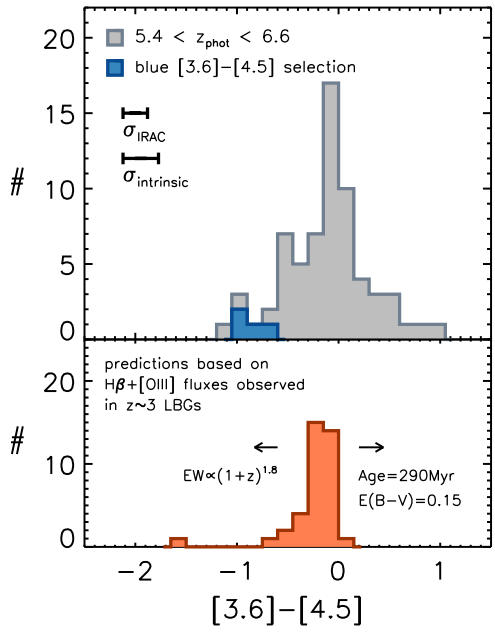

Figure 6. Top panel: the [3.6] − [4.5] color distribution (gray histogram) of sources with photometric redshifts (from the *HST* photometry) within the redshift range $z \sim 5.4 - 6.6$ (68% confidence) where [O III] contributes to the 3.6 μm flux, while Hα contributes to the 4.5 μm flux. Sources that satisfy our ultra-blue IRAC selection criterion (Equation (2)), but prefer a $z < 6.6$ are indicated with the blue histogram (note that for a few sources the very blue [3.6] − [4.5] colors are not significant). The upper error bar on the left side of the panel indicates the scatter in the [3.6] − [4.5] color distribution due to photometric uncertainty in the IRAC bands. The lower error bar indicates the intrinsic scatter, as calculated from the observed scatter and the simulated IRAC uncertainties. Bottom panel: the predicted [3.6] − [4.5] color distribution (orange histogram) using the [O III] and Hβ EWs as measured by Schenker et al. (2013b) and Holden et al. (2014) in $z \sim 3$ LBGs with the MOSFIRE spectrograph. We predict the [3.6] − [4.5] color assuming Case B recombination and a flat continuum in f_ν. Evolution of the EW strength as a function of redshift (e.g., Smit et al. 2014) will broaden the [3.6] − [4.5] color distribution and at the same time shift the median color of the distribution to bluer values as indicated by the left black arrow on the panel. The right black arrow indicates the shift in [3.6] − [4.5] color when we assume a somewhat more evolved stellar population with an age of 290 Myr and a dust content of $E(B-V) = 0.15$ (see Section 4.2 for details).

[3.6] − [4.5] colors if similar sources are present at $z \sim 6$. We computed the predicted [3.6] − [4.5] colors from the observed [O III]λ4959,5007 Å EW and an estimate of the Hα EW derived from the Hβ EW, assuming case B recombination and a flat continuum in f_ν. For $([3.6] - [4.5])_{\rm continuum} = 0$ and assuming all sources are at $z = 6$, the [O III] and Hβ EWs allow for a direct calculation of the [3.6] − [4.5] colors such as shown in the bottom panel of Figure 6.

The spread in colors in the predicted distribution is smaller than the spread in the observed distribution at $z \sim 6.0$. Even when accounting for the spread in [3.6] − [4.5] due to the observational uncertainties in the IRAC bands, the intrinsic spread exceeds the width of the predicted distribution (see the error bars in the top panel of Figure 6). However, this is likely explained by the spread in the color of the underlying continuum emission due to different dust content and ages of the galaxies in the observed distribution, while we assumed a fixed flat continuum in f_ν for our predicted colors. A somewhat evolved population (∼300 Myr) and modest dust content ($E(B-V) \sim 0.15$) could redden the IRAC color of some of the observed galaxies by $\Delta([3.6] - [4.5]) \sim 0.2$ (see Figure 6). Similarly, the [3.6] − [4.5] color of the continuum can be as blue as −0.4 mag for a very young ($\lesssim$10 Myr) and dust-free galaxy.

Another effect that can change the predicted [3.6] − [4.5] color distribution is a probable evolution of the emission line EWs between $z \sim 3$ and $z \sim 6$, e.g., because we are observing increasingly younger generations of galaxies. Assuming all line EWs follow the evolution of the Hα EW derived by Fumagalli et al. (2012) for star-forming galaxies in the redshift range $z \sim 0 - 2$, the predicted spread in [3.6] − [4.5] color would increase, while the median predicted [3.6] − [4.5] color would be bluer by $\Delta([3.6] - [4.5]) = 0.23$.

From the above comparison we conclude that the blue [3.6] − [4.5] sources at $z \sim 6.0$ (indicated with the blue histogram in the top panel of Figure 6) can be explained by the high [O III]/Hβ values observed in $z \sim 3$ LBGs and a blue continuum [3.6] − [4.5] color as seen in young galaxies with low dust content and low metallicity, possibly in combination with an evolving EW strength of nebular emission lines as a function of redshift.

5. A FIDUCIAL SAMPLE OF $z \sim 6.8$ EMISSION LINE GALAXIES

In this section we will present a strategy for the efficient use of *HST*+IRAC information to select galaxies over the redshift range $z \sim 6.6 - 6.9$. In Section 4.1 we showed that sources at $z \sim 6.6 - 6.9$ have very blue [3.6] − [4.5] colors and that we can use this information to significantly reduce the uncertainty on

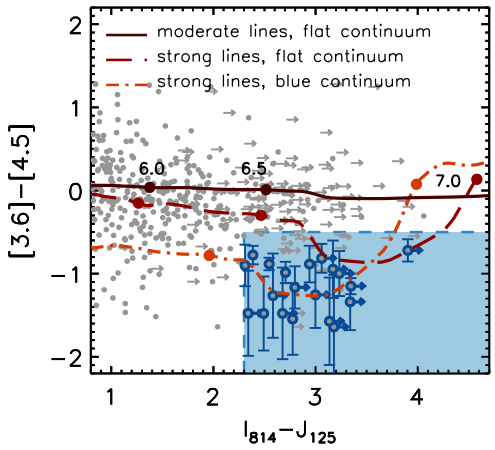

Figure 7. Color–color diagram showing the selection criteria for our fiducial $z \sim 6.8$ sample (blue shaded region) with the color measurements of galaxies from our base as a sample of $z \sim 5-8$ galaxies over all five CANDELS fields (gray points and arrows; non-detections in the I_{814} band are placed at the 1σ upper limit). The blue encircled points indicate the 20 selected sources listed in Table 1, that satisfy our blue IRAC criterion (Equation (2)) as well as a $I_{814} - J_{125} > 2.3$ (see Section 5) criterion (sources that have large uncertainties in the IRAC color are not selected). The solid lines indicate tracks for three different galaxy templates as described in Figure 3, with the solid points indicating the colors of the templates at $z = [6.0, 6.5, 7.0]$.

the redshift determination. However, we also found that a small number of galaxies at $z < 6.6$ show extremely blue colors as well and we cannot distinguish these sources from galaxies in the redshift range $z \sim 6.6-6.9$ on the basis of the [3.6] − [4.5] IRAC colors alone.

5.1. Selection of Our Fiducial $z \sim 6.8$ Sample

To effectively exclude $z \sim 6$ galaxies from our selection of galaxies in the narrow redshift range $z \sim 6.6-6.9$, we require an additional selection criterion besides our [3.6] − [4.5] color cut (Equation (2)). For our fiducial sample we require that sources show a significant break across the I_{814} and J_{125} bands:

$$I_{814} - J_{125} > 2.3. \quad (3)$$

If I_{814} is undetected we use the 1σ upper limit to compute the color. This dropout criterion should effectively exclude the $z < 6.5$ contaminating galaxies from our target $z \sim 6.8$ selection (see Figure 7). We will separately select $z \sim 6$ ultra-blue galaxies using a $I_{814} - J_{125} < 2.3$ criterion.

We apply the criteria given by Equations (2) and (3) to our photometric catalogs of sources in all five CANDELS fields (Bouwens et al. 2014) and find 20 sources in our fiducial $z \sim 6.8$ sample and 8 sources that are likely at lower redshift. We summarize the properties of the fiducial sample and the sources that satisfy Equation (2) but not Equation (3) in Table 1, and we show postage stamps of the sources in Figures 8 and 9. The typical width of the 68% redshift confidence intervals for the sources in our fiducial sample as given by $P(z_{\rm phot}, HST + {\rm IRAC})$ is $\Delta z = 0.2$.

5.2. Ascertaining the Mean Redshift and Contamination Fraction of the $z \sim 6.8$ Sample

To test the robustness of our selection we stacked the sources from GOODS-N/S selected by Equations (2) and (3) and we show the resulting SED in Figure 10. We estimate the mean redshift for our selected sources from the stacked photometry. We emphasize that we do not use our flux measurements in the I_{814}, 3.6 and 4.5 μm bands, due to flux measurements in these bands playing an important role in the selection of the sources themselves; this should ensure that our derived redshift is not significantly biased by the selection process itself. We find a photometric redshift of $z_{\rm phot} = 6.81^{+0.25}_{-0.28}$, consistent with the redshift range $z \sim 6.6-6.9$. Since the measured flux in the J_{125} band was also used in the selection of individual sources, it could have a minor effect on the estimated redshift for the stacked photometry. Excluding the J_{125}-band flux measurements in deriving the best-fit redshift, gives a photometric redshift of $z_{\rm phot} = 6.77 \pm 0.31$.

As a test of the robustness of our blue IRAC selection criterion (Equation (2)) against scatter in the [3.6] − [4.5] color due to the uncertainties in the 3.6 and 4.5 μm flux measurements, we simulated the photometric scatter assuming an intrinsic IRAC color [3.6] − [4.5] = 0 for all sources from the five CANDELS fields in our $z \sim 5-8$ base sample. We simulated the observed colors by adding noise to the 3.6 and 4.5 μm-band fluxes, that match the measured flux uncertainties (1000× per source). From this simulation we conclude that less than 0.1 source with an intrinsic IRAC color [3.6] − [4.5] = 0 has scattered into our fiducial selection over all five CANDELS fields.

The only significant source of interlopers to our fiducial sample of $z \sim 6.8$ galaxies would seem to arise from galaxies at $z < 6.6$. To quantify this interloper fraction, we first estimate the fraction of ultra-blue [3.6] − [4.5] sources at $z < 6.6$ from Figure 6, which is 6%. From the bottom panel of Figure 3 (see also Table 1) we find that sources in our fiducial sample have estimated redshifts as far as $\Delta z \sim 0.3$ away from our desired redshift range $z \sim 6.6-6.9$. We therefore assume that $z \sim 6.3-6.6$ galaxies cannot be completely removed from our fiducial sample using our $I_{814} - J_{125} < 2.3$ color criterion (Equation (3)) and could potentially be contaminating our $z \sim 6.8$ sample. Multiplying those sources from our base sample of galaxies from all five CANDELS fields (Section 2.3) with $z_{\rm phot}$, *HST* $\sim$ 6.3 – 6.6 by the 6% fraction with ultra-blue IRAC colors, we estimate that ∼2.0 sources could have scattered into our fiducial $z \sim 6.8$ sample from $z < 6.6$. We therefore conservatively estimate that ∼90% of the 20 sources with extreme IRAC colors and $I_{814} - J_{125}$ colors > 2.3 (Table 1) lie in the redshift range $z \sim 6.6-6.9$.

Furthermore, comparing the 20 galaxies from our $z \sim 6.8$, IRAC ultra-blue sample (90% of which we estimated to lie in this redshift range: see previous paragraph) with the 35 galaxies estimated to lie in the redshift range $z \sim 6.6-6.9$ from the redshifts of our $z \sim 5-8$ base sample, we estimate that ∼50% of all sources at $z \sim 6.8$ exhibit ultra-blue colors (versus 6% at $z \sim 6$). This makes IRAC ultra-blue sources roughly ∼8 times more common at $z \sim 6.8$ than at $z < 6.6$. This is useful to establish, since it indicates that ultra-blue IRAC criteria—such as we propose—reduce the numbers of contaminants in our samples significantly, i.e., improving the purity of $z \sim 6.6$–6.9 selections by a factor of 8 over what one would manage using *HST* and ground-based observations alone.

5.3. Quantifying the Rest-frame EWs of [O III]+Hβ in our $z \sim 6.8$ IRAC Ultra-blue Sample

Using the assumption that the 4.5 μm band is free of emission line contamination at $z \sim 6.6-6.9$ while the 3.6 μm band is contaminated by [O III] and Hβ, we can make a

Table 1
Properties of Extremely Blue [3.6] − [4.5] Galaxies in Our Samples

ID	R.A.	Decl.	m_{H160}	$I_{814}-J_{125}$	[3.6] − [4.5]	$z^{c}_{\rm phot,HST}$	$z^{c}_{\rm phot,HST+IRAC}$	EW([O III]+Hβ)[Å]
Fiducial $z\sim6.8$ Sample[a]								
GND-7035815571	12:37:03.586	+62:15:57.18	26.3 ± 0.1	>3.2	−1.0 ± 0.3	$7.26^{+0.33}_{-0.34}$	$6.81^{+0.07}_{-0.07}$	1374 ± 415
GND-7025017221	12:37:02.500	+62:17:22.17	26.8 ± 0.1	>2.8	−1.2 ± 0.3	$7.25^{+0.43}_{-0.45}$	$6.76^{+0.06}_{-0.06}$	1779 ± 486
GND-6427518385	12:36:42.753	+62:18:38.55	27.0 ± 0.2	2.5 ± 0.9	−1.5 ± 0.4	$6.52^{+0.37}_{-0.37}$	$6.71^{+0.08}_{-0.06}$	2591 ± 1095
GND-6372717115	12:36:37.279	+62:17:11.59	26.3 ± 0.1	>3.2	−0.9 ± 0.3	$6.75^{+0.27}_{-0.26}$	$6.70^{+0.13}_{-0.12}$	1193 ± 485
GSD-2504846559[l]	03:32:50.481	−27:46:55.95	25.8 ± 0.1	2.3 ± 0.9	−0.9 ± 0.2	$6.83^{+0.32}_{-0.34}$	$6.78^{+0.08}_{-0.08}$	962 ± 293
GSD-2254450533	03:32:25.443	−27:50:53.36	26.3 ± 0.1	>3.3	−1.3 ± 0.3	$6.96^{+0.26}_{-0.26}$	$6.78^{+0.06}_{-0.06}$	1471 ± 432
GSD-2237749136	03:32:23.778	−27:49:13.64	26.6 ± 0.1	>3.0	−1.3 ± 0.4	$6.90^{+0.20}_{-0.19}$	$6.74^{+0.09}_{-0.09}$	1800 ± 704
GSD-2252146266[l]	03:32:25.216	−27:46:26.69	26.9 ± 0.1	>3.1	−1.6 ± 0.5	$6.94^{+0.23}_{-0.23}$	$6.75^{+0.06}_{-0.06}$	2424 ± 1083
COS-3731073631	10:00:37.310	+02:27:36.31	26.0 ± 0.1	>2.3	−1.5 ± 0.5	$7.43^{+1.07}_{-1.23}$	$6.68^{+0.14}_{-0.14}$	1686 ± 676
COS-2987030247[d]	10:00:29.870	+02:13:02.47	24.8 ± 0.1	2.7 ± 0.8	−1.0 ± 0.1	$6.99^{+1.16}_{-1.25}$	$6.66^{+0.14}_{-0.14}$	1128 ± 166
COS-1318939512[e]	10:00:13.189	+02:23:9.512	25.0 ± 0.1[e]	2.8 ± 1.0	−1.5 ± 0.4	$7.15^{+1.07}_{-0.99}$	$6.75^{+0.09}_{-0.08}$	786 ± 301
COS-3018555981[f]	10:00:30.185	+02:15:59.81	24.9 ± 0.1	>3.3	−1.2 ± 0.1	$7.76^{+0.79}_{-0.82}$	$6.76^{+0.07}_{-0.07}$	1424 ± 143
EGS-4434164969	14:19:44.341	+52:56:49.69	26.3 ± 0.1	>2.6	−1.3 ± 0.5	$7.08^{+1.41}_{-1.82}$	$6.62^{+0.19}_{-0.20}$	1321 ± 619
EGS-5711424617	14:19:57.114	+52:52:46.17	25.1 ± 0.1	2.4 ± 0.2	−0.8 ± 0.1	$6.33^{+0.22}_{-0.21}$	$6.47^{+0.10}_{-0.10}$	927 ± 149
EGS-3506853076[g]	14:19:35.068	+52:55:30.76	26.2 ± 0.1	2.9 ± 0.9	−0.9 ± 0.2	$7.18^{+0.94}_{-0.82}$	$6.62^{+0.16}_{-0.16}$	1084 ± 298
EGS-1952445714[h]	14:19:19.524	+52:44:57.14	25.3 ± 0.1	>3.9	−0.7 ± 0.1	$7.52^{+0.66}_{-0.66}$	$6.75^{+0.11}_{-0.11}$	768 ± 151
EGS-1350184593[l]	14:19:13.501	+52:48:45.93	26.5 ± 0.1	>3.2	−1.6 ± 0.6	$7.56^{+0.71}_{-0.74}$	$6.72^{+0.09}_{-0.08}$	2391 ± 1196
EGS-2713432218	14:19:27.134	+52:53:22.18	26.1 ± 0.1	>3.1	−0.8 ± 0.2	$7.56^{+0.66}_{-0.68}$	$6.71^{+0.13}_{-0.14}$	1048 ± 242
UDS-0089122444	02:17:00.891	−05:12:24.44	26.5 ± 0.2	>2.7	−1.5 ± 0.6	$7.34^{+0.83}_{-0.87}$	$6.70^{+0.11}_{-0.10}$	2620 ± 1350
UDS-5754844803[i]	02:17:57.548	−05:08:44.80	24.8 ± 0.2	2.5 ± 1.1	−0.9 ± 0.1	$7.05^{+1.08}_{-1.28}$	$6.61^{+0.19}_{-0.17}$	915 ± 95
$z\sim6.0$ Sample[b]								
GND-6322718286	12:36:32.273	+62:18:28.67	26.2 ± 0.1	2.0 ± 0.4	−1.1 ± 0.3	$7.01^{+0.23}_{-0.24}$	$6.75^{+0.08}_{-0.09}$ [j]	…
GNW-6390808452	12:36:39.080	+62:08:45.29	26.1 ± 0.2	2.1 ± 0.8	−0.7 ± 0.1	$5.87^{+0.33}_{-0.33}$	$4.84^{+1.50}_{-0.03}$ [k]	…
GSD-2234402156	03:32:23.449	−27:50:21.56	26.5 ± 0.1	1.5 ± 0.3	−1.0 ± 0.3	$5.97^{+0.22}_{-0.22}$	$6.09^{+0.13}_{-0.12}$ [k]	…
GSW-2573853217	03:32:57.381	−27:53:21.78	26.2 ± 0.2	>1.7	−0.8 ± 0.2	$6.27^{+0.25}_{-0.26}$	$6.46^{+0.13}_{-0.13}$ [k]	…
ERS-2115344329	03:32:11.539	−27:44:32.99	26.9 ± 0.1	1.1 ± 0.2	−1.0 ± 0.4	$5.84^{+0.25}_{-0.30}$	$6.03^{+0.12}_{-0.21}$ [k]	…
EGS-2802701763	14:20:28.027	+53:00:17.63	26.5 ± 0.2	1.1 ± 0.3	−1.4 ± 0.5	$5.48^{+0.54}_{-0.84}$	$5.94^{+0.14}_{-0.24}$ [k]	…
UDS-5417745460	02:17:54.177	−05:14:54.60	25.5 ± 0.1	2.2 ± 0.4	−0.7 ± 0.2	$6.32^{+0.29}_{-1.23}$	$6.45^{+0.18}_{-0.19}$ [k]	…
UDS-5125213373	02:17:51.252	−05:11:33.73	25.6 ± 0.1	1.8 ± 0.3	−0.9 ± 0.3	$6.01^{+0.34}_{-1.36}$	$6.25^{+0.14}_{-0.15}$ [k]	…

[a] In addition to our blue IRAC criterion (see Equation (2)) we require $I_{814}-J_{125}>2.3$ for our fiducial 6.6–6.9 sample. If I_{814} is undetected we use the 1σ upper limit to compute the color.
[b] Here, we list sources with $I_{814}-J_{125}<2.3$, as well as blue IRAC colors (satifying Equation (2)). Low S/N sources cannot unambiguously be selected in the $z\sim6.0$ sample, i.e., if they satisfy $I_{814}-J_{125}<2.3\ \wedge\ {\rm S/N}(I_{814})<1$. However, this is only the case for one source in our sample, i.e., GSW-2573853217. The photometric redshift estimate of this source indicates that it likely belongs in the $z\sim6.0$ sample.
[c] Error bars indicate the 68% confidence interval.
[d] In the stacked ground-based optical image (inverse variance weighted) this source is detected at 7.9 ± 1.5 nJy. However, this flux appears to derive from a foreground source, close to our object of interest but distinctly separated in the *HST* optical images.
[e] This source is detected at the edge of the *HST*/WFC3 field of view. We have verified that this source is also detected in the ground-based photometry from the UltraVISTA survey (see Ilbert et al. 2013). However, the total magnitude for this source measured from ground-based data appears to be somewhat fainter than we measure for *HST*, suggesting that our *HST* stack might be affected by some non-Gaussian noise.
[f] This source was independently discovered by Tilvi et al. (2013) and Bowler et al. (2014), who estimated a photometric redshift of $7.24^{+0.38}_{-0.25}$ and $6.77^{+0.14}_{-0.19}$ respectively.
[g] This source is only marginally resolved; while its spatial profile and SED are much more consistent with its being a $z\sim6.8$ galaxy, we cannot completely exclude the possibility that it is a low-mass star.
[h] Though the size of this source is consistent with its being a low-mass star, the SED of this source is better fit by a high-redshift galaxy than a stellar tempate.
[i] This source, better known as 'Himiko' (Ouchi et al. 2009, 2013), has a spectroscopic redshift at $z_{Ly\alpha}=6.59$, consistent with our photometric redshift estimate within the 68% probability window.
[j] This source is weakly detected in I_{814} with $I_{814}-J_{125}=2.0\pm0.4$ and therefore included in the $z\sim6$ sample. However, due to a $<1\sigma$ detection in the z_{850} band, our estimated photometric redshift indicates a $z\sim6.75$ solution.
[k] The typical uncertainty in $z_{\rm phot}$, *HST* + IRAC for this $z\sim6$ sample is very small. The ultra-blue IRAC colors of these galaxies are preferentially fit by the template with the most extreme [O III]/Hα ratio, which allows for little variation of the colors of the continuum emission and thereby narrows the redshift probability distribution. However, the shape of the spectral energy distributions of these galaxies (and the range of [O III]/Hα ratios at $z\sim6$) is unknown, and therefore it is likely that the width of the redshift probability distribution is underestimated for this particular sample.
[l] The 4.5 μm images for these candidates require a modest (∼50%) correction for contaminating flux from neighboring sources. While we would expect the corrections we perform to be generally quite accurate, we flag these candidates as somewhat less robust than the other candidates in our sample.

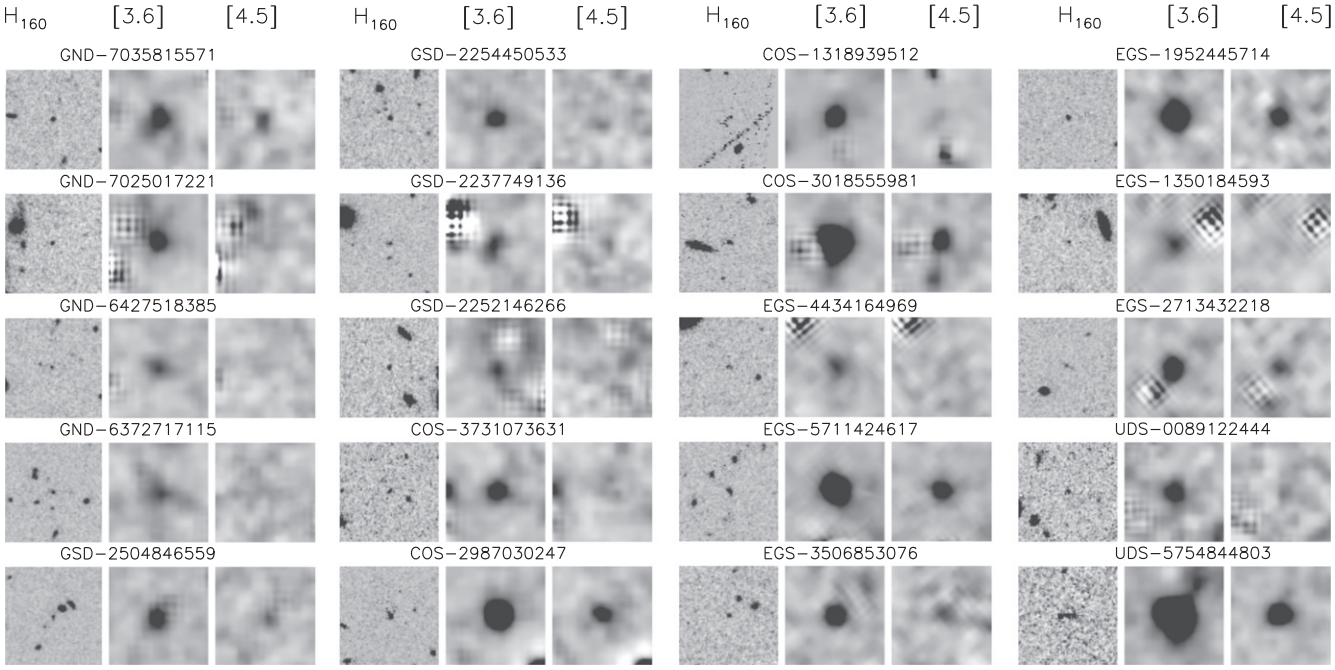

Figure 8. *HST* H_{160}, *Spitzer*/IRAC 3.6, and 4.5 μm band postage stamp negative images ($8\farcs4 \times 8\farcs4$) of our fiducial sample of galaxies at $z \sim 6.8$ in the CANDELS fields with extremely blue [3.6] − [4.5] IRAC colors (satisfying Equation (2)) and $I_{814} - J_{125} > 2.3$ (see Section 5). The IRAC postage stamps have been cleaned for contamination from neighboring sources (see Section 2.2). Properties of the sources are listed in Table 1.

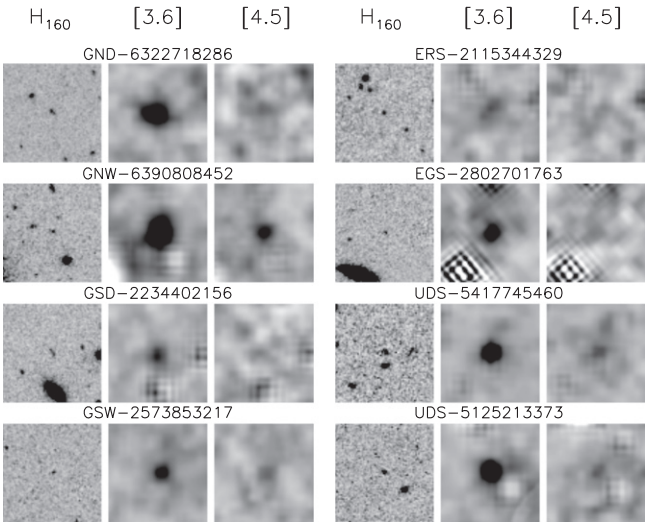

Figure 9. *HST* H_{160}, *Spitzer*/IRAC 3.6, and 4.5 μm band postage stamp negative images ($8\farcs4 \times 8\farcs4$) of our sample of galaxies at $z \sim 6.0$ in the CANDELS fields with extremely blue [3.6] − [4.5] IRAC colors (satisfying Equation (2)) and $I_{814} - J_{125} < 2.3$ (see Section 5). The IRAC postage stamps have been cleaned for contamination from neighboring sources (see Section 2.2). Properties of the sources are listed in Table 1.

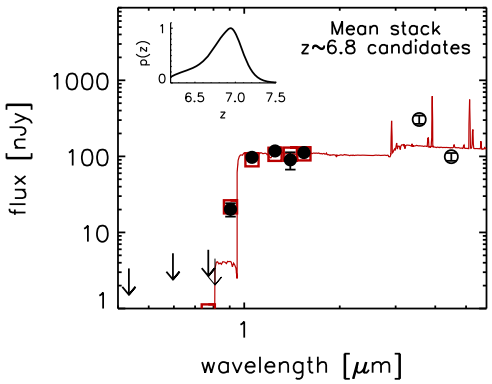

Figure 10. Template fit to the stacked broadband observations of blue [3.6] − [4.5] galaxies (Equation (2)) that also satisfy $I_{814} - J_{125} > 2.3$ (see Section 5). Fluxes and upper limits (black points and thick arrows) show the mean *HST* photometry (error bars obtained from bootstrapping). We do not include the stacked I_{814}, 3.6 and 4.5 μm band flux measurements (indicated by the thin arrow and open black points) in this analysis in order to avoid biasing our photometric redshift due to our use of the $I_{814} - J_{125}$ and [3.6] − [4.5] colors in selecting the sources. The inset panel shows the probability distribution on the mean redshift for our sample. This distribution has a mean value of $z_{\rm phot} = 6.81^{+0.25}_{-0.28}$, consistent with the desired redshift range for our selection.

prediction of the [O III] strength and estimate the fraction of high-EW [O III] emitters in the high redshift galaxy population. The median [3.6] − [4.5] color of our $z \sim 6.8$ sample is −1.2 ± 0.3, indicating a typical rest-frame EW$_0$([O III]+H β) > 1000 Å (see Smit et al. 2014).

In order to obtain a more accurate estimate of the [O III] EW, we calculated the difference between the contaminated 3.6 μm flux and an estimate of the rest-frame optical continuum flux. The continuum flux was estimated by fitting the SEDs of the galaxies with stellar population templates using the Fitting and Assessment of Synthetic Templates code (Kriek et al. 2009). In the fitting procedure we used stellar population templates by Bruzual & Charlot (2003) and constant star formation histories with ages between 30 Myr and the age of the universe at $z = 6.6$. We assumed a Salpeter (1955) IMF with limits 0.1–100 $M_\odot$ and a Calzetti et al. (2000) dust law. We considered dust contents between $A_V = 0 - 1.5$ and subsolar metallicities between 0.2 and 0.4 $Z_\odot$. We only considered the *HST* and the 4.5 μm IRAC photometry in deriving our best-fit model, while excluding the measured 3.6 μm fluxes (due to their being impacted by the [O III]+Hβ lines). We used the best fit templates from our fitting procedure to obtain an estimate of

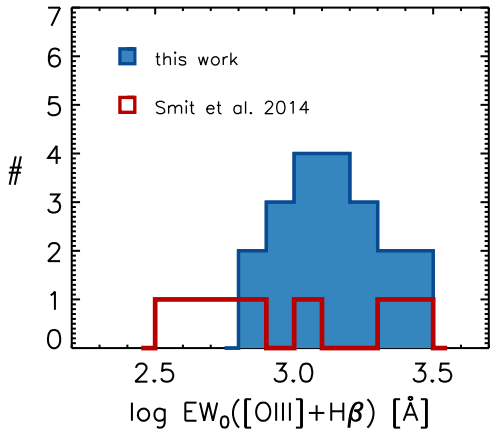

Figure 11. Rest-frame EW distribution of [O III]+Hβ (blue filled histogram), estimated from the sources in our $z \sim 6.8$ sample (see Section 5.3). For reference we show the EWs of the sources from Smit et al. (2014) that were selected on their photometric redshift being in the range $z \sim 6.6 - 7.0$ (red histogram). In Section 5.2 we calculated that our fiducial sample roughly selects the ~50% strongest line emitters at $z \sim 6.8$. The observed median of the distribution is 1375 Å rest-frame EW, but correcting for the bias in the measurement due to scatter in the [3.6] − [4.5] color (for details see Section 5.3) we estimate a median EW$_0$([O III]+Hβ) of 1085 Å. The excellent agreement between our sample and the 50% most extreme sources from Smit et al. (2014) provides further evidence that high-EW nebular emission lines are indeed ubiquitous at high redshift.

the 3.6 μm continuum flux and from this we derived the rest-frame EW of the combined [O III]λ4959,5007 Å+Hβ lines.

Our estimates of rest-frame EW$_0$([O III]+Hβ) are listed in Table 1 and range from ~900 to >2000 Å with a median of 1375 Å. Though the uncertainties on the EWs are too large for the >2000 Å EW measurements to be secure, we estimate rest-frame EWs as high as $\gtrsim$1000 Å in the majority of our selected sources. Nevertheless, we note that the median EW we derive here will be biased toward high values because we are using the same [3.6] − [4.5] color measurements to derive the EWs as we used for the selection. We estimate this bias by investigating the selection process in a distribution of galaxies with an intrinsic IRAC color [3.6] − [4.5] = 0 and simulated the noise in the 3.6 and 4.5 μm bands based on the measured flux uncertainties. We selected 50% of the sources with the bluest simulated [3.6] − [4.5] colors (in agreement with our estimates in Section 5.2) and found these sources have a median [3.6] − [4.5] = −0.15. Using this color bias and Equations (1) and (2) from Smit et al. (2014) and assuming a flat continuum in f_ν for these sources, we estimate an observed bias of ~290 Å on the measured [O III]+Hβ EW of 1375 Å due to the noise in the IRAC bands. This suggests that the median EW of our selected sources is really 1085 Å in the noise-free case.

We show the predicted EW$_0$([O III]+Hβ) distribution of our $z \sim 6.8$ sample in Figure 11. We compare this distribution with the EW distribution from the seven lensed sources selected in the redshift range $z \sim 6.6 - 7.0$ reported by Smit et al. (2014) and comparable intrinsic UV luminosities. We use the same procedure to derive EWs for these sources as described in the paragraph above. For one source we use the 1σ upper limit due to the high uncertainties in the IRAC photometry. The comparison between the two distributions confirms that our suggested critera for selecting $z \sim 6.8$ sources rougly selects the ~50% most extreme line emitters at that redshift.

The median UV–luminosity of our sample (computed from the H_{160}-band fluxes and assuming $z = 6.75$) is $M_{\rm UV} = -20.66$, roughly comparable to the $M^*_{\rm UV} = -20.87 \pm 0.26$ from the $z \sim 7$ luminosity function derived by Bouwens et al. (2014). Combining this information with our calculation in Section 5.2 we argue that roughly ~50% of the $M^*_{\rm UV}$ galaxy population at $z \sim 7$ produces extreme nebular emission lines (EW$_0$([O III]+H β) $\gtrsim$ 1000 Å) in the rest-frame optical.

It is interesting to compare these derived EWs to the observed [O III]+Hβ EW distribution at $z \sim 3$ reported by Schenker et al. (2013b) and Holden et al. (2014). In order to match our $z \sim 6.8$ sample, we use only the 50% most extreme emitters from the combined Schenker et al. (2013b) and Holden et al. (2014) samples and calculate a median EW$_0$([O iii] + Hβ) = 390 Å (with a median redshift $z \sim 3.5$). Comparing this number to the mean EW at $z \sim 6.8$ and assuming the evolution of nebular emission line EWs scales as $\sim(1+z)^n$ (see Fumagalli et al. 2012), we derive EW$_0$([OIII]+Hβ) $\propto (1+z)^{1.9\pm0.36}$. This slope is consistent with the slope derived by Fumagalli et al. (2012) for Hα EWs over the redshift range $z \sim 0 - 2$ ($n \sim 1.8$) but somewhat steeper than the slope derived by Labbé et al. (2013), who found $n = 1.2 \pm 0.25$ over the redshift range $z \sim 1 - 8$.

6. SUMMARY AND DISCUSSION

In this paper we explore the use of IRAC colors to select star-forming galaxies in the narrow redshift range $z \sim 6.6 - 6.9$. Sources in this redshift range are expected to be very blue due to the boosted flux in the 3.6 μm band from high-EW [O III] emission, while the 4.5 μm band is free from contamination of strong nebular emission lines. This suggests that a blue IRAC criterion may be appropriate for selecting galaxies in the redshift range $z \sim 6.6 - 6.9$.

In evaluating the suitability of such a selection criterion we analyze a large sample of LBGs in GOODS-N and GOODS-S with relatively high S/N *Spitzer*/IRAC coverage from the *Spitzer* GOODS, ERS, and S-CANDELS programs (Ashby et al. 2015). We find that the majority of candidates with extremely blue [3.6] − [4.5] colors are consistent with $z \sim 6.8$. In addition to the $z \sim 6.6 - 6.9$ sources, we also find a small number of sources with extreme [3.6] − [4.5] colors more likely to be at $z \sim 6.0$. The blue [3.6] − [4.5] galaxies at $z \sim 6.0$ can be explained by high [OIII]/Hβ ratios, such as those found in $z \sim 3$ LBGs (Schenker et al. 2013b; Holden et al. 2014), lensed galaxies at $z \sim 1 - 2$ (Brammer et al. 2012b; van der Wel et al. 2013), and in Green Pea galaxies at $z \sim 0$ (Amorín et al. 2012; Jaskot & Oey 2013) in combination with blue colors for the optical continuum.

To obtain a clear selection in the redshift range $z \sim 6.6 - 6.9$, we suggest the use of ultra-blue IRAC colors combined with an $I_{814} - J_{125} > 2.3$ dropout criterion. Based on our analysis in Section 5, we estimate that at least 90% of the sources selected by these criteria lie in the redshift range $z \sim 6.6 - 6.9$. We systematically apply such criteria to our source catalogs from the five CANDELS fields (720 arcmin^2) and find 20 sources (~0.03 arcmin^{-2}). A comparison with the total number of galaxies from our catalogs in this redshift range suggests that we select the ~50% bluest IRAC sources at $z \sim 6.8$ at a typical UV–luminosity $M_{\rm UV} \sim M^*_{\rm UV,\ z=7}$.

We estimate a median uncertainty on the redshift estimates for our fiducial sources of $\Delta z = 0.2$ (68% confidence). Such redshift uncertainties are significantly smaller than one finds for these objects without the inclusion of the IRAC fluxes. For example, we find a median 68% confidence interval on $z_{\rm phot}$, *hst* of $\Delta z = 0.6$ and $\Delta z = 1.7$, respectively, for sources in GOODS-N/S and COSMOS/EGS/UDS. Among other uses, such tight constraints on the redshifts are necessary for efficient observations with ALMA. Our constraints on the redshift of these sources means that we should typically only require two ALMA tunings to successfully observe [C II]λ157.7 μm in band 6.

Using our fiducial sample of $z \sim 6.8$ sources with ultra-blue $[3.6]-[4.5]$ colors, we estimate the strength of [O III] λ4959,5007 Å+Hβ from the contaminated 3.6 μm flux. We find that the majority of the sources in our sample show EWs as high as EW$_0$([O III]+H β) $\gtrsim$ 1000 Å, in excellent agreement with the ∼50% most extreme sources from Smit et al. (2014).

Given the recent study by Stark et al. (2014a), who found evidence for strong [O III]$\lambda\lambda$4959,5007 Å emission in sources with high-EW [C III]λ1908 Å lines at $z \sim 2$, it seems reasonable to suppose that our strong [O III] emitters also exhibit relatively strong [C III] lines, and therefore our sources are excellent targets for follow-up studies with near-IR spectroscopy (e.g., Stark et al. 2014b).

Finally, with the future launch of the *JWST*, we will be able to target these extreme line-emitter galaxies with *JWST*'s near-infrared spectrograph (NIRSpec). The [O III]λ5007 Å line in a typical galaxy from our sample should be detected at 10σ in the *JWST*/NIRSpec $R = 100$ mode with a mere 60 s exposure.

We thank Jarle Brinchmann, Rob Crain, Paul van der Werf, and Tim van Kempen for useful discussions. We are grateful to Brad Holden for providing us with the complete catalog from Holden et al. (2014). We thank the anonymous referee of our paper for valuable feedback on our manuscript. We acknowledge support from ERC grant HIGHZ #227749, and an NWO vrij competitie grant.

REFERENCES

Amorín, R., Pérez-Montero, E., Vílchez, J. M., & Papaderos, P. 2012, ApJ, 749, 185
Anders, P., & Fritze-v. Alvensleben, U. 2003, A&A, 401, 1063
Ashby, M. L. N., Willner, S. P., Fazio, G. G., et al. 2013, ApJ, 769, 80
Ashby, M. L. N., Willner, S. P., Fazio, G. G., et al. 2015, ApJS, submitted
Beckwith, S. V. W., Stiavelli, M., Koekemoer, A. M., et al. 2006, AJ, 132, 1729
Bertin, E., & Arnouts, S. 1996, A&AS, 117, 393
Bouwens, R. J., Illingworth, G. D., Franx, M., et al. 2009, ApJ, 705, 936
Bouwens, R. J., Illingworth, G. D., Oesch, P. A., et al. 2011, ApJ, 737, 90
Bouwens, R. J., Illingworth, G. D., Oesch, P. A., et al. 2012, ApJ, 754, 83
Bouwens, R. J., Illingworth, G. D., Oesch, P. A., et al. 2013, ApJ, 793, 115
Bouwens, R. J., Illingworth, G. D., Oesch, P. A., et al. 2014, ApJ, submitted (arXiv:1403.4295)
Bowler, R. A. A., Dunlop, J. S., McLure, R. J., et al. 2012, MNRAS, 426, 2772
Bowler, R. A. A., Dunlop, J. S., McLure, R. J., et al. 2014, MNRAS, 440, 2810
Bradley, L. D., Trenti, M., Oesch, P. A., et al. 2012, ApJ, 760, 108
Brammer, G. B., van Dokkum, P. G., & Coppi, P. 2008, ApJ, 686, 1503
Brammer, G. B., van Dokkum, P. G., Franx, M., et al. 2012, ApJS, 200, 13
Brammer, G. B., Sánchez-Janssen, R., Labbé, I., et al. 2012, ApJL, 758, L17
Bruzual, G., & Charlot, S. 2003, MNRAS, 344, 1000
Capak, P., Aussel, H., Ajiki, M., et al. 2007, ApJS, 172, 99
Carilli, C. L., & Walter, F. 2013, ARA&A, 51, 105
Caruana, J., Bunker, A. J., Wilkins, S. M., et al. 2014, MNRAS, 443, 2831
Coe, D., Benítez, N., Sánchez, S. F., et al. 2006, AJ, 132, 926
Calzetti, D., Armus, L., Bohlin, R. C., et al. 2000, ApJ, 533, 682
Curtis-Lake, E., McLure, R. J., Dunlop, J. S., et al. 2013, MNRAS, 429, 302
Dunlop, J. S., McLure, R. J., Robertson, B. E., et al. 2012, MNRAS, 420, 901
Dunlop, J. S., Rogers, A. B., McLure, R. J., et al. 2013, MNRAS, 432, 3520
Ellis, R. S., McLure, R. J., Dunlop, J. S., et al. 2013, ApJL, 763, L7
Eyles, L. P., Bunker, A. J., Stanway, E. R., et al. 2005, MNRAS, 364, 443
Eyles, L. P., Bunker, A. J., Ellis, R. S., et al. 2007, MNRAS, 374, 910
Finkelstein, S. L., Papovich, C., Salmon, B., et al. 2012, ApJ, 756, 164
Finkelstein, S. L., Papovich, C., Dickinson, M., et al. 2013, Natur, 502, 524
Fumagalli, M., Patel, S. G., Franx, M., et al. 2012, ApJL, 757, L22
Furusawa, H., Kosugi, G., Akiyama, M., et al. 2008, ApJS, 176, 1
González, V., Labbé, I., Bouwens, R. J., et al. 2010, ApJ, 713, 115
González, V., Labbé, I., Bouwens, R. J., et al. 2011, ApJL, 735, L34
González, V., Bouwens, R. J., Labbé, I., et al. 2012, ApJ, 755, 148
González, V., Bouwens, R., Illingworth, G., et al. 2014, ApJ, 781, 34
Grogin, N. A., Kocevski, D. D., Faber, S. M., et al. 2011, ApJS, 197, 35
Holden, B. P., Oesch, P. A., Gonzalez, V. G., et al. 2014, ApJ, submitted (arXiv:1401.5490)
Holwerda, B. W., Trenti, M., Clarkson, W., et al. 2014, ApJ, 788, 77
Ilbert, O., McCracken, H. J., le Fèvre, O., et al. 2013, A&A, 556, A55
Illingworth, G. D., Magee, D., Oesch, P. A., et al. 2013, ApJS, 209, 6
Jaskot, A. E., & Oey, M. S. 2013, ApJ, 766, 91
Juneau, S., Dickinson, M., Bournaud, F., et al. 2013, ApJ, 764, 176
Kewley, L. J., Dopita, M. A., Leitherer, C., et al. 2013, ApJ, 774, 100
Kirkpatrick, J. D., Cushing, M. C., Gelino, C. R., et al. 2011, ApJS, 197, 19
Koekemoer, A. M., Faber, S. M., Ferguson, H. C., et al. 2011, ApJS, 197, 36
Kotulla, R., Fritze, U., Weilbacher, P., & Anders, P. 2009, MNRAS, 396, 462
Kriek, M., van Dokkum, P. G., Labbé, I., et al. 2009, ApJ, 700, 221
Labbé, I., Bouwens, R., Illingworth, G. D., & Franx, M. 2006, ApJL, 649, L67
Labbé, I., González, V., Bouwens, R. J., et al. 2010, ApJL, 716, L103
Labbé, I., González, V., Bouwens, R. J., et al. 2010, ApJL, 708, L26
Labbé, I., Oesch, P. A., Bouwens, R. J., et al. 2013, ApJL, 777, L19
Laporte, N., Streblyanska, A., Clement, B., et al. 2014, A&A, 562, L8
Lorenzoni, S., Bunker, A. J., Wilkins, S. M., et al. 2011, MNRAS, 414, 1455
McLure, R. J., Dunlop, J. S., Bowler, R. A. A., et al. 2013, MNRAS, 432, 2696
Oesch, P. A., Bouwens, R. J., Illingworth, G. D., et al. 2012, ApJ, 745, 110
Oesch, P. A., Bouwens, R. J., Illingworth, G. D., et al. 2013, ApJ, 773, 75
Oesch, P. A., Bouwens, R. J., Illingworth, G. D., et al. 2014, ApJ, 786, 108
Oke, J. B., & Gunn, J. E. 1983, ApJ, 266, 713
Ouchi, M., Ono, Y., Egami, E., et al. 2009, ApJ, 696, 1164
Ouchi, M., Ellis, R., Ono, Y., et al. 2013, ApJ, 778, 102
Pentericci, L., Fontana, A., Vanzella, E., et al. 2011, ApJ, 743, 132
Salmon, B., Papovich, C., Finkelstein, S. L., et al. 2015, ApJ, 799, 183
Salpeter, E. E. 1955, ApJ, 121, 161
Schaerer, D., & de Barros, S. 2009, A&A, 502, 423
Schenker, M. A., Ellis, R. S., Konidaris, N. P., & Stark, D. P. 2013, ApJ, 777, 67
Schenker, M. A., Ellis, R. S., Konidaris, N. P., & Stark, D. P. 2014, ApJ, 795, 20
Schenker, M. A., Robertson, B. E., Ellis, R. S., et al. 2013, ApJ, 768, 196
Shim, H., Chary, R.-R., Dickinson, M., et al. 2011, ApJ, 738, 69
Sirianni, M., Jee, M. J., Benítez, N., et al. 2005, PASP, 117, 1049
Skelton, R. E., Whitaker, K. E., Momcheva, I. G., et al. 2014, ApJS, 214, 24
Smit, R., Bouwens, R. J., Labbé, I., et al. 2014, ApJ, 784, 58
Stanway, E. R., McMahon, R. G., & Bunker, A. J. 2005, MNRAS, 359, 1184
Stark, D. P., Ellis, R. S., Bunker, A., et al. 2009, ApJ, 697, 1493
Stark, D. P., Ellis, R. S., Chiu, K., Ouchi, M., & Bunker, A. 2010, MNRAS, 408, 1628
Stark, D. P., Richard, J., Siana, B., et al. 2014a, MNRAS, 445, 3200
Stark, D. P., Richard, J., Charlot, S., et al. 2014b, MNRAS, arXiv:1408.3649
Stark, D. P., Schenker, M. A., Ellis, R., et al. 2013, ApJ, 763, 129
Steidel, C. C., Adelberger, K. L., Giavalisco, M., Dickinson, M., & Pettini, M. 1999, ApJ, 519, 1
Steidel, C. C., Rudie, G. C., Strom, A. L., et al. 2014, ApJ, 795, 165
Szalay, A. S., Connolly, A. J., & Szokoly, G. P. 1999, AJ, 117, 68
Tilvi, V., Papovich, C., Tran, K.-V. H., et al. 2013, ApJ, 768, 56
Treu, T., Schmidt, K. B., Trenti, M., Bradley, L. D., & Stiavelli, M. 2013, ApJL, 775, L29
van der Wel, A., van de Ven, G., Maseda, M., et al. 2013, ApJL, 777, L17
Vanzella, E., Fontana, A., Pentericci, L., et al. 2014, A&A, 569, AA78
Wilkins, S. M., Bunker, A. J., Stanway, E., Lorenzoni, S., & Caruana, J. 2011, MNRAS, 417, 717
Wilkins, S. M., Coulton, W., Caruana, J., et al. 2013, MNRAS, 435, 2885
Windhorst, R. A., Cohen, S. H., Hathi, N. P., et al. 2011, ApJS, 193, 27
Yabe, K., Ohta, K., Iwata, I., et al. 2009, ApJ, 693, 507
Yan, H., Dickinson, M., Giavalisco, M., et al. 2006, ApJ, 651, 24
Yan, H., Dickinson, M., Stern, D., et al. 2005, ApJ, 634, 109